

Spin-Dynamics of the antiferromagnetic $S=1/2$ -Chain at finite magnetic Fields and intermediate Temperatures

S. Grossjohann and W. Brenig
*Institut für Theoretische Physik, TU Braunschweig,
 38106 Braunschweig, Germany*

(Dated: November 4, 2018)

We present a study of the dynamic structure factor of the antiferromagnetic spin-1/2 Heisenberg chain at finite temperatures and finite magnetic fields. Using Quantum-Monte-Carlo based on the stochastic series expansion and Maximum-Entropy methods we evaluate the longitudinal and the transverse dynamic structure factor from vanishing magnetic fields up to and above the threshold B_c for ferromagnetic saturation, as well as for high and for intermediate temperatures. We study the field-induced redistribution of spectral weight contrasting longitudinal versus transverse excitations. At finite fields below saturation incommensurate low-energy modes are found consistent with zero temperature Bethe-Ansatz. The crossover between the field induced ferromagnet above B_c and the Luttinger liquid below B_c is analyzed in terms of the transverse spin-dynamics. Evaluating sum-rules we assess the quality of the analytic continuation and demonstrate excellent consistency of the Maximum-Entropy results.

PACS numbers: 75.10.Jm, 75.40.Gb, 75.50.Ee, 75.40.Mg

I. INTRODUCTION

The antiferromagnetic spin-1/2 Heisenberg chain (AFHC) is one of the most intensively studied strongly correlated quantum many body systems. In the presence of an external magnetic field, its generalization to anisotropic exchange, the XXZ model, reads

$$H = J \sum_l [S_l^z S_{l+1}^z + \frac{\Delta}{2} (S_l^+ S_{l+1}^- + S_l^- S_{l+1}^+) - B S_l^z], \quad (1)$$

where J is the antiferromagnetic exchange interaction with an anisotropy ratio Δ , $S_l^{\pm,z}$ are the spin operators on site l of the chain, and $B = g\mu_B \hbar H$ is the magnetic field. From a materials perspective SrCuO_2^1 ($J/k_B \approx 2600\text{K}$), $\text{Sr}_2\text{CuO}_3^{2,3,4}$ ($J/k_B \approx 2200\text{K}$), and $\text{Cu}(\text{C}_4\text{H}_4\text{N}_2)(\text{NO}_3)_2^5$ ($J/k_B \approx 10.7\text{K}$) are topical examples of both, low- and high- J AFHC compounds which have been studied intensively⁶. Recently, dynamical correlation functions of the AFHC have become accessible to a variety of high resolution spectroscopies at finite temperature and in the presence of external magnetic fields, eg. inelastic neutron scattering (INS)⁷, high-field nuclear magnetic resonance (NMR)^{8,9,10,11}, muon spin-resonance (μSR)¹², and magnetic transport^{13,14}.

The AFHC is integrable, including the cases of $h \neq 0$ and $\Delta \neq 1$. Bethe-Ansatz (BA)^{15,16} has been used to investigate its ground state properties. Static thermodynamic quantities, eg. the specific heat, the magnetic susceptibility and the magnetization have been investigated by several methods including thermodynamic BA, Quantum Monte Carlo (QMC), as well as transfer-matrix and density-matrix renormalization (DMRG) group, see^{17,18,19} and refs. therein.

Fractionalization of the spin excitations into multi spinon states is a fingerprint of the AFHC^{20,21}. At zero

temperature, $T = 0$, numerical analysis of these excitations has been carried out in many studies using exact diagonalization (ED) of finite AFHCs, see eg. refs.^{22,23,24}, including the effects of h and Δ , as well as by dynamical variants the DMRG^{25,26}. In principle, also BA allows to determine dynamical correlation functions, however calculating the corresponding matrix elements is highly non-trivial and progress has been made only recently. By now analytic expressions for dynamical spin correlation functions are available for the two-^{27,28,29} and the four-spinon sector^{30,31,32,33} at $\Delta = 1$, $h = 0$ and $T = 0$. In addition, determinant approaches^{34,35} allow for numerical treatment of two-^{36,37,38} and many-spinon^{39,40} states of the XXZ chain in finite magnetic fields, at $T = 0$. Finally, mapping to field theory in the continuum limit⁴¹ has been used to study the small- q behavior of longitudinal dynamical structure factor in the gapless regime^{42,43,44}.

At finite temperatures, the dynamical correlations functions of the AFHC remain an open issue. The dynamical structure factor $S^{\alpha\beta}(q, \omega)$ has been studied by complete ED of small systems^{45,46} in the context of spin diffusion, see^{13,47} and refs. therein. However, such analysis is limited by finite size effects to $k_B T \gtrsim J$. Recently, finite temperature real-time auto- and next-nearest neighbor correlation functions have been accessed by DMRG methods^{48,49}. However, the time range of such calculations is limited, as the spectrum of the reduced density matrix used to truncate the Hilbert space becomes dense. In this respect QMC remains a key tool to evaluate the $S^{\alpha\beta}(q, \omega)$, for system sizes which are close to the thermodynamic limit, over the complete Brillouin zone, and at finite temperatures, with the limitations set primarily by the analytic continuation of imaginary-time data⁵⁰. QMC analysis of $S^{\alpha\beta}(q, \omega)$ has been carried out for $h = 0$ ^{51,52,53}, results for $h \neq 0$, however, are lacking.

The purpose of this work is to shed more light

the finite-temperature dynamical structure factor of the AFHC in the presence of external magnetic fields using QMC. The paper is organized as follows. In section II we briefly summarize the QMC approach we use. Section III we analyze the transverse and longitudinal structure factor versus temperature and magnetic field. In section IV we consider several sum rules of the AHFC. We summarize and conclude in section V.

II. METHODS

In this paper we present results for the Fourier transform of the dynamic structure factor

$$S^{\alpha\beta}(q, \omega) = \int_{-\infty}^{\infty} dt e^{i\omega t} S^{\alpha\beta}(q, t), \quad (2)$$

where t refers to real time and $S^{\alpha\beta}(q, t) = \langle S_q^\alpha(t) S_{-q}^\beta \rangle$ with $S_q^\alpha = \sum_r e^{-iqr} S_r^\alpha$ being the spin component α at momentum q . In the following we discuss both, the *longitudinal* and the *transverse* structure factor, i.e. $\alpha\beta = zz$ and $\alpha\beta = xx$. These components are directly accessible to unpolarized neutron scattering. Other types of transverse components, eg. $\alpha\beta = +-$ require polarized neutrons and will not be considered here⁵⁴. For $\alpha\beta = xx(zz)$ $S^{\alpha\beta}(q, \omega)$ is related to the imaginary time structure factor $S^{\alpha\beta}(q, \tau) = \langle S_q^\alpha(\tau) S_{-q}^\beta \rangle$ through the integral transform

$$S^{\alpha\beta}(q, \tau) = \frac{1}{\pi} \int_0^\infty d\omega K(\omega, \tau) S^{\alpha\beta}(q, \omega) \quad (3)$$

with the kernel $K(\omega, \tau) = e^{-\tau\omega} + e^{-(\beta-\tau)\omega}$.

The imaginary time correlation functions $S^{\alpha\beta}(q, \tau)$ will be evaluated by QMC. Here we employ the stochastic series expansion (SSE) introduced by Sandvik *et al.*⁵⁵. This method is based on a particular form of the high temperature series expansion of the partition function which can be sampled efficiently⁵⁶. To this end, the Heisenberg model is rewritten in terms of N_b bond operators

$$H = -J \sum_{b=0}^{N_b} (H_{1,b} + H_{2,b}) \quad (4)$$

where $H_{1,b} = 1/2 - S_b^z S_{b+1}^z$ and $H_{2,b} = (S_b^+ S_{b+1}^- + S_b^- S_{b+1}^+)/2$ refer to the *diagonal* and *off-diagonal* parts of H within the S^z basis. Within this notation the partition function is

$$Z = \sum_\alpha \sum_n \sum_{S_n} \frac{(-\beta)^n}{n!} \langle \alpha | \prod_{k=1}^n H_{a_k, b_k} | \alpha \rangle \quad (5)$$

where $|\alpha\rangle = |S_1^z, \dots, S_N^z\rangle$ refers to the S^z basis and S_n

$$S_n = [a_1, b_1][a_2, b_2] \dots [a_n, b_n] \quad (6)$$

is an index for the *operator string* $\prod_{k=1}^n H_{a_k, b_k}$, labeling each specific product of operators where $a_k \in \{1, 2\}$ and $b_k \in \{1, \dots, N_b\}$.

The operator string is subject to importance sampling by a Metropolis scheme, splitted into two different types of updates: a *diagonal* update which changes the number of diagonal operators H_{1,b_k} in the operator string and a cluster type update which performs changes of the type $H_{1,b_k} \leftrightarrow H_{2,b_k}$. On bipartite lattices the latter, so-called *loop* update guarantees an even number of off-diagonal operators H_{2,b_k} in the expansion. This ensures positiveness of the transition probabilities.

Imaginary time spin-correlation functions $S_{i,j}^{\alpha\beta}(\tau) = \langle e^{\tau H} S_i^\alpha e^{-\tau H} S_j^\beta \rangle$, for $\tau \in [0, \beta)$, and lattice sites i, j can also be sampled by the SSE using that⁵⁷

$$S_{i,j}^{\alpha\beta}(\tau) = \left\langle \sum_{m=0}^n \frac{\tau^m (\beta - \tau)^{n-m} n!}{\beta^n (n-m)! m!} \bar{C}_{i,j}^{\alpha\beta}(m) \right\rangle_W \quad (7)$$

where, in contrast to the thermal average $\langle \dots \rangle$, the brackets $\langle \dots \rangle_W$ with subscript W refer to averaging over operator string configurations with weights generated by the Metropolis scheme. The quantity $\bar{C}_{i,j}^{\alpha\beta}(m)$ in eqn. (7) is the static real space correlation function

$$\bar{C}_{i,j}^{\alpha\beta}(m) = \frac{1}{n+1} \sum_{p=0}^n S_i^\alpha(p) S_j^\beta(p+m) \quad (8)$$

which, in the case $\alpha\beta = zz$, can be measured within the diagonal or slightly more efficient within the loop update⁵⁸ where $m, p \leq n$ refer to positions within the operator string and $S_i^\alpha(p)$ refers at the intermediate state $|\alpha(p)\rangle = \prod_{k=1}^p H_{a_k, b_k} |\alpha\rangle$ of the expansion. Transverse correlations $\alpha\beta = xx, +- , -+$ in a code working in the S^z basis can only be accessed by following the loop within the extended configuration space (see⁵⁸). Finally, the Fourier transform $S^{\alpha\beta}(q, \tau) = \sum_j e^{-iqj} S_{j,0}^{\alpha\beta}(\tau)/N$ is used as input for the inversion problem eqn. (3).

Extracting $S^{\alpha\beta}(q, \omega)$ from eqn. (3) is notoriously complicated because of the QMC noise and the singular nature of $K(\omega, \tau)$. However, this problem can be handled successfully by Maximum Entropy methods. Here we use Bryan's algorithm⁵⁹ which is specifically designed for over-sampled data sets and therefore well-suited to treat QMC results. For details we refer the reader to the Appendix.

III. RESULTS

In this chapter we will present results for the transverse and longitudinal dynamic structure factor at finite temperatures, in the range of $T = J/20 \dots J$ and magnetic fields below and above the saturation field B_c . All QMC calculations refer to systems with 128 sites, typically with one billion Monte-Carlo updates (one diagonal and sufficient⁵⁶ loop updates), distributed over 1000 bins. Only 50-100 τ -points were extracted for each temperature in order to prevent over-sampling of the relatively short expansion orders at elevated temperatures close to

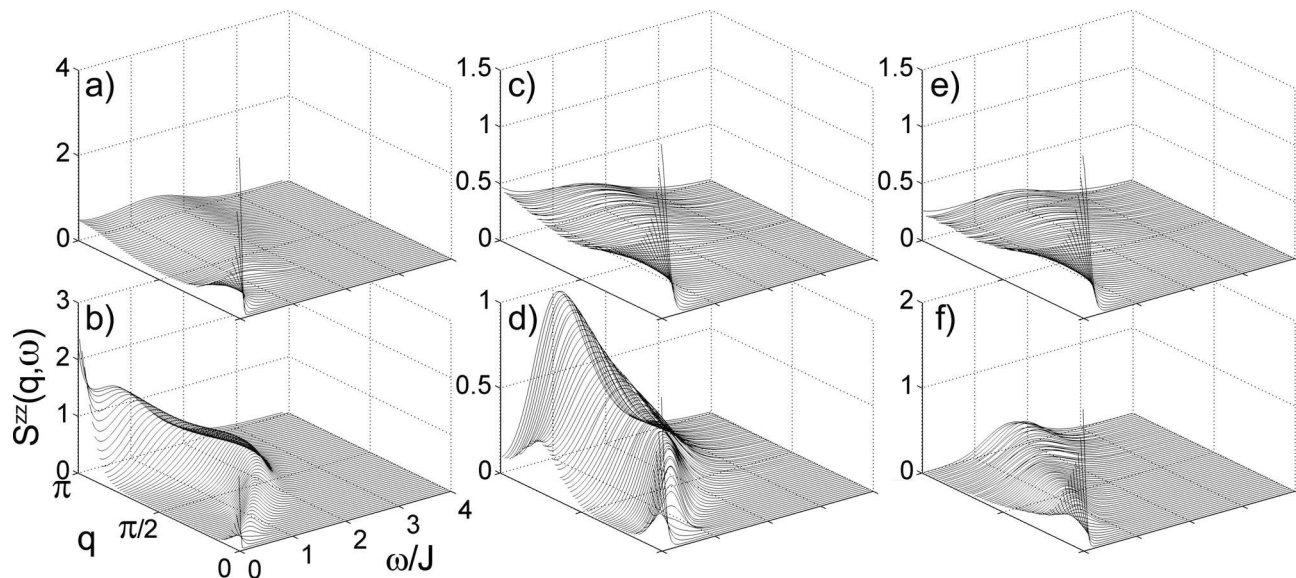


FIG. 1: 3D plot of the longitudinal dynamic structure factor by QMC + MaxEnt as function of frequency ω and wave vector q . Temperatures and magnetic field in units J : a) $T=1$ and $B=0$, b) $T=0.25$ and $B=0$, c) $T=1$ and $B=1$, d) $T=0.25$ and $B=1$, e) $T=1$ and $B=2$ and f) $T=0.25$ and $B=2$.

$T = J$. An indication for over-sampling is given by diagonalizing the covariance matrix which exhibits vanishing eigenvalues in case of statistically dependent data.

A. Longitudinal Dynamic Structure Factor $S^{zz}(q, \omega)$

In Fig. 1 and 2 we show the longitudinal dynamic structure factor both, as a 3D and a contour plot for two different temperatures $T = \{J, J/4\}$ and three different magnetic fields $B = \{0, B_c/2, B_c\}$. The solid lines displayed in the contour plots for $B < B_c$ refer to the upper and lower boundaries of the two-spinon spectrum as obtained from BA selection rules²². For zero magnetic field they enclose a region which, within 2-spinon calculations, contains about 73% of the zero temperature spectral weight²⁸. We will now focus on each of the magnetic fields separately.

1. The case $B = 0$

At zero magnetic field and high temperatures, i.e. Figs. 1a) and 2a), we find a strong broadening of spectral features. While the region of finite spectral weight remains bounded from above by $J\pi \sin|q/2|$ ⁶⁰, significant weight appears below the lower two-spinon boundary $\frac{\pi J}{2} \sin|q|$ set by de Cloizeaux-Pearson⁶¹. Most notably, high spectral weight occurs for $q, \omega \rightarrow 0$. This intensity is related to spin conservation which dominates the long wave-length dynamics in the quasi-classical regime $k_B T \gg J$. The question whether the long wave-length spin dynamics in the AFHC can be described by spin

diffusion is a long-standing issue with no final answer as of today. For a recent review on the present status and related references we refer to¹³.

Unfortunately QMC is too sensitive to the default model for the MaxEnt continuation in the small- q, ω regime⁵² to elucidate the issue of spin-diffusion. Yet, we would like to mention agreement of our results regarding the frequency-transformed autocorrelation function $S_0^{zz}(\omega)$, i.e. the q -integrated dynamic structure factor (not shown within this work) with previous QMC, performed at $B = 0$, high temperature series expansion⁵³ and TMRG⁴⁹. These results exhibit a $\omega^{-0.3\dots-0.4}$ -divergent behaviour which bears resemblance to the phenomenological approaches by Bloembergen⁶² and de Gennes⁶³ who predicted $\omega^{-1/2}$.

Next we consider lower temperatures, i.e. $T = J/4$. As is obvious from Figs. 1b) and 2b), spectral weight is removed from the long wave-length regime in this case. Both figures demonstrate that most of the spectral weight is confined within the two-spinon boundaries with however still an appreciable intensity below the lower boundary. This is consistent with findings reported in⁵². In contrast to $T = J$ we find a strongly enhanced spectral weight at $q = \pi$ owing to the increase of the antiferromagnetic correlation length⁶⁴ which is consistent with the autocorrelation function reported in ref.⁴⁹.

In the limit $(q, \omega) \rightarrow (\pi, 0)$ we find indications for diverging behaviour of $S^{zz}(\pi, \omega)$ with decreasing temperatures. This is shown in more detail in Fig. 3, scanning a wide range of temperatures from $T = J$ to $T = J/20$. As can be seen, the spectrum consists of an upturn for $\omega \rightarrow 0$ and a peak at finite ω . The latter peak shifts to lower energies while gaining sharpness as $T \rightarrow 0$. For

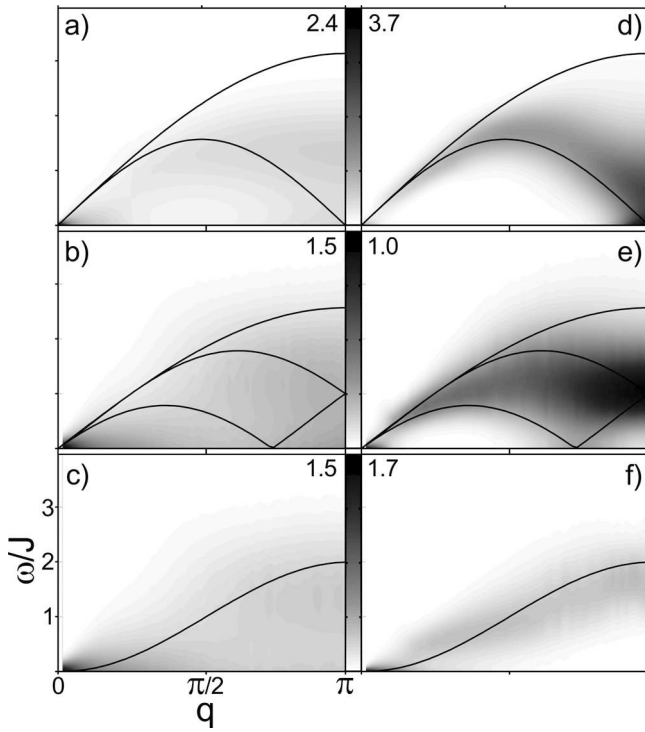


FIG. 2: Contour plot of the longitudinal dynamic structure factor as function of frequency ω and wave vector q . Temperatures and magnetic fields in units of J : a) $T=1$ and $B=0$, b) $T=0.25$ and $B=0$, c) $T=1$ and $B=1$, d) $T=0.25$ and $B=1$, e) $T=1$ and $B=2$ and f) $T=0.25$ and $B=2$. For $B < B_c$ the solid lines are zero temperature excitation boundaries by the Müller-ansatz²² while at critical fields the exact zero temperature $1 - \cos(q)$ dispersion⁷⁰ is shown.

$T \rightarrow 0$, Fig. 3 suggest that the peak will merge with the zero- ω upturn to form a single divergence at $\omega \rightarrow 0$, as predicted by 2-spinon calculations at $T = 0$ which lead to $S^{zz}(\pi, \omega) \sim \omega^{-1.22}$. A similar peak at finite ω was observed also in ref.⁵². However, smaller systems sizes in that case, i.e. $N = 32$, render the zero- ω upturn into a shoulder only. Biasing the default model by several sum-rules, it was shown in ref.⁵², that $S^{zz}(\pi, \omega)$ on 32-site systems could be obtained with only a single peak at finite ω . Recent SSE-QMC on 128-site systems at $B = 0$ show only a single rounded maximum, centered at $\omega = 0$ ⁵³. While all these findings are consistent with the formation of a zero- ω divergence as $T \rightarrow 0$, they show that the details of the low- ω spectrum are subject to details of the MaxEnt approach. Nevertheless, we will detail later that our results are consistent with several sum-rules, including those which are particularly sensitive to the low frequency behavior of the spectrum.

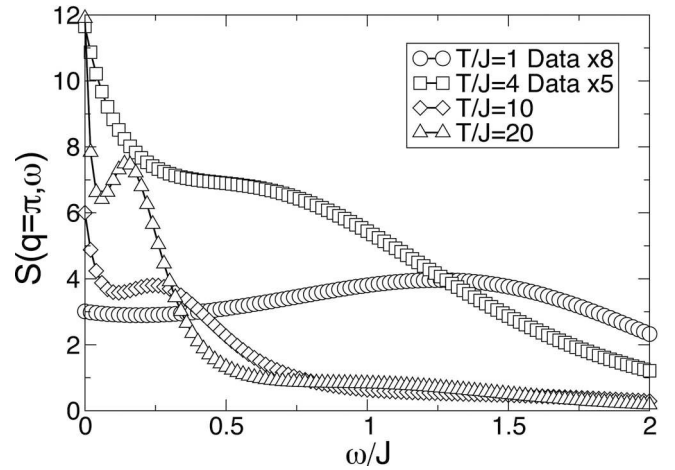


FIG. 3: Zero-field dynamic structure factor at $q = \pi$ for four different temperatures (in units of J) $\{1, 0.25, 0.1, 0.05\}$. As the temperature decreases we find an increased divergent behaviour for $\omega \rightarrow 0$ as predicted by 2-spinon calculations. In addition there is a low frequency peak which shifts to lower energies while steadily gaining sharpness. Note that the dataset for $T = 1$ and for $T = 0.25$ was multiplied by a factor of eight, respectively five for illustrative reasons.

2. The case $B = B_c/2$

Figs. 1, 2 c) and d) depict the longitudinal structure factor at half of the critical field. The impact of a finite magnetic field is fourfold. First, at zero momentum the longitudinal structure factor is proportional to the square of the field-induced magnetization at zero frequency, i.e. $S^{zz}(q = 0, \omega) \sim \langle S^z \rangle^2 \delta(\omega)$. To focus on the remaining spectrum, we have chosen to skip the single wave vector $q = 0$ in all 3D, as well as contour plots of $S^{zz}(q, \omega)$ for $B \neq 0$. Second, longitudinal excitations with $q \neq 0$ will have decreasing matrix elements with increasing magnetic field. This is consistent with the evolution of the overall scale in Fig. 1 a)-e) and b)-f). Third, longitudinal spin-excitations at the zone boundary are energetically unfavorable in a magnetic field. In fact, at low temperatures a gap can be observed at $q = \pi$, which is proportional to the magnetic field²² (see Fig. 2 d)). Finally, a soft mode occurs at an incommensurable wave vector $q_s = \pi(1 - 2\langle S^z \rangle)$ (see Fig. 2 d)). This can be understood in terms of the Jordan-Wigner fermionic description of the AFHC^{65,66,67}, where S_q^z is related to the fermion density and the magnetic field plays the role of a chemical potential driving incommensurability. This finding is consistent with ref.²², with interacting spin-wave calculation⁶⁸ as well with finite system diagonalization⁶⁹. The role of temperature is evident. At high temperatures, i.e. $T = J$ in Fig. 2 c), $S^{zz}(q, \omega)$ is rather featureless and extends clearly beyond the boundaries set by the two-spinon continuum. This changes as the temperature is lowered to $T = J/4$, Fig. 2 d), where the spectrum is far more confined to within the dCP

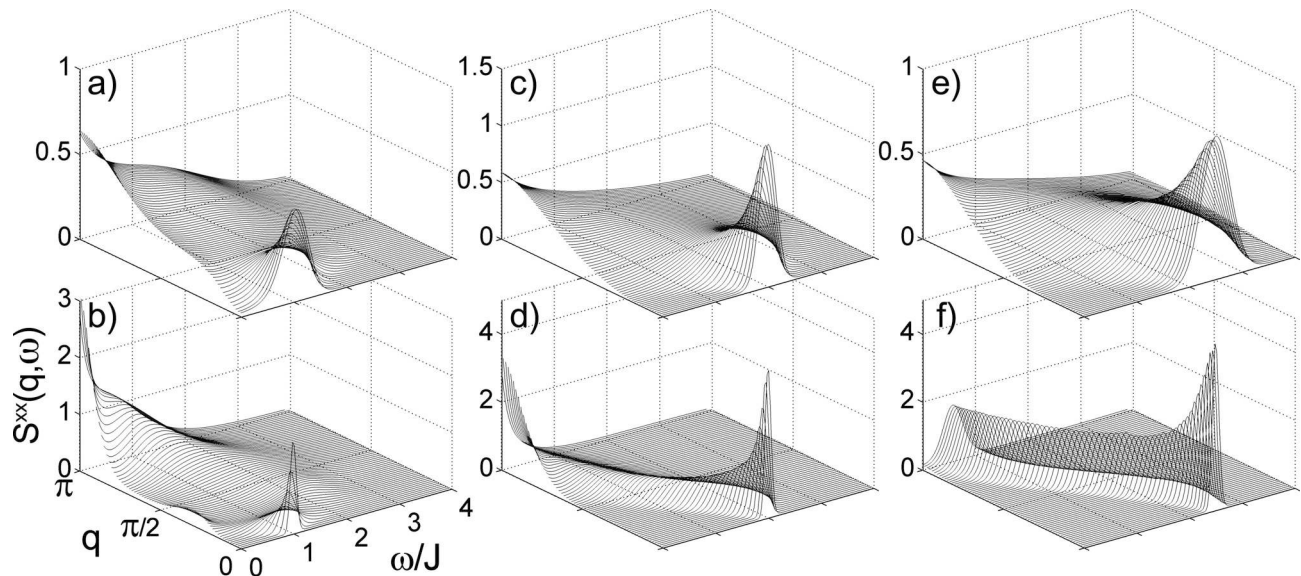


FIG. 4: Transverse dynamic structure factor by QMC + MaxEnt as function of frequency ω and wave vector q . Temperature and magnetic field in units of J : a) $T=1$ and $B=1$, b) $T=0.25$ and $B=1$, c) $T=1$ and $B=2$, d) $T=0.25$ and $B=2$, e) $T=1$ and $B=2.5$ and f) $T=0.25$ and $B=2.5$.

boundaries and displays more pronounced features. In particular, the weight is enhanced as $(q, \omega) \rightarrow (\pi, J)$.

3. The case $B = B_c$

For $B \geq B_c$ and $T = 0$, the statistical operator of the AFHC is pure and corresponds to the fully polarized state, i.e. $S^{zz}(q, \omega) = N(1/4) \delta_{q,0} \delta(\omega)$. Additional finite spectral weight for $q, \omega \neq 0$ will occur only for $T > 0$. To observe this we have again removed the wave vector $q = 0$ from Figs. 1, 2 e), f), which are at the critical field. Indeed, on lowering the temperature from panel e) to panel f) in Fig. 1, the remaining total spectral weight decreases. Apart from this the higher temperature spectrum is rather featureless, while the lower temperature spectrum clearly resembles the exact zero temperature dispersion of $(1 - \cos(q))^{70}$ (see Fig. 2 f)). This excitation has a constant spectral weight $2\pi/N$ for $q \neq 0$, which vanishes in the thermodynamic limit.

B. Transverse dynamic structure factor $S^{xx}(q, \omega)$

In Fig. 4 and 5 we show the transverse dynamic structure factor as 3D and as contour plots for identical temperatures $T/J = \{1, 0.25\}$ as for the longitudinal dynamic structure factor, however for a different range of magnetic fields $B/J = \{1, 2, 2.5\}$. For vanishing magnetic field we refer to Figs. 1, 2 a), b) for $S^{xx}(q, \omega)$ which is identical to $S^{zz}(q, \omega)$ at $B = 0$ due to $SU(2)$ invariance.

1. The case $B = B_c/2$

First, we note that the results for $S^{xx}(q, \omega)$ in Figs. 4, 5 a) and b) are clearly different from those for $S^{zz}(q, \omega)$ in Figs. 1, 2 c) and d) at identical magnetic fields. This is to be expected, since the application of a finite magnetic field breaks the $SU(2)$ invariance of the AFHC. Second, long-wave transverse spin-excitations will experience the Zeeman energy due to the magnetic field, which leads to a spin gap of size B/J at $q = 0$. This has to be contrasted against the gap at $q = \pi$ in $S^{zz}(q, \omega)$ at finite fields in Figs. 1, 2 d). Third, and as for the longitudinal case a field driven zero mode at $q = q_s$ can be seen in 2 a), b) - with a rather low intensity as $T \rightarrow 0$. In contrast to the longitudinal case, this mode develops out of the zone center and moves to the zone boundary with $q_s = 2\pi \langle S^z \rangle^{22,71,72}$.

Even though it can be misleading to compare MaxEnt data based on different QMC data sets quantitatively due to the underlying different statistic quality, we notice enhanced spectral weight near the zone boundary in Fig. 4 b) compared to zero magnetic field in Fig. 1 b), which means that a weak uniform field strengthens the antiferromagnetic order in the transverse structure factor. This effect was also observed in²² for small fields and by Karbach *et al.* within the static structure factors⁷³.

2. The case $B \geq B_c$

At intermediate fields selection rules²² allow for a fairly complex distribution of spectral weight as is also obvious from the solid lines in Figs. 5 a) and b). In contrast to

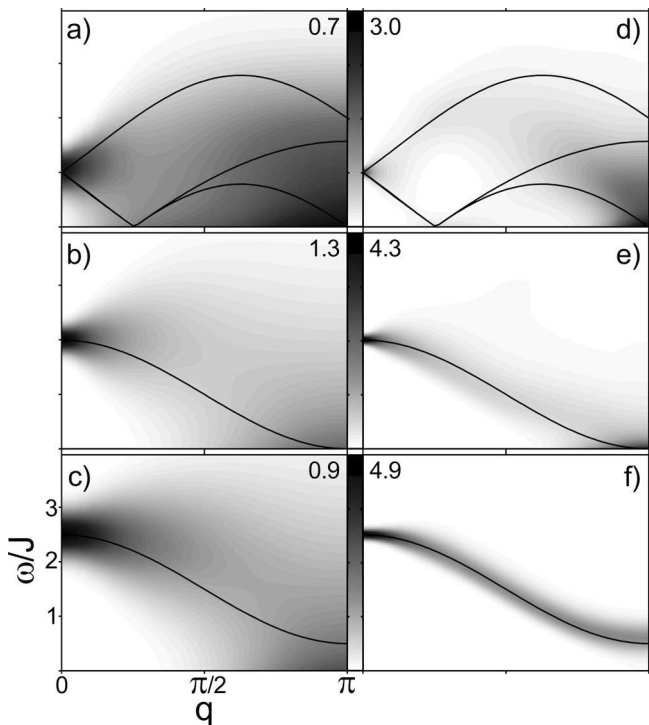


FIG. 5: Transverse dynamic structure factor by QMC + MaxEnt as function of frequency ω and wave vector q in a contour plot. For parameter details see text or Fig. 4. The solid lines for half critical field a) and b) are zero temperature excitation boundaries of different BA selection rules (see²²). For $B \geq B_c$ the one-magnon cosine dispersion is shown.

this, above the saturation field and at low temperatures, a straightforward picture emerges (see Fig. 4,5 d) and f)). In this regime and for $T \rightarrow 0$ the systems is fully polarized. In that case the elementary excitations are non-interacting ferromagnetic one-magnon states, leading to a dispersion $E(k) = J \cos(k) + B$ in the transverse structure factor, with a momentum-independent spectral weight²². For finite T , we find that this picture is modified in two ways. First, significant thermal broadening occurs, which as e.g. in Fig. 5 e), at $B = 2.5$ and $T = J$ can lead to a complete closure of the zone boundary spin-gap. Second, and as can be seen in Figs. 4 d) and f), there is a substantial wave-vector dependence of the spectral weight in the cosine-signature of the one-magnon state. The latter is due to the elementary one-magnon states being excited in a polarized background which contains thermal fluctuations⁵⁴. Finally, we emphasize the difference in the evolution of the overall spectral weight, contrasting longitudinal versus transverse excitations. While in Fig. 1 the weight of the excitations decreases with increasing field, this is not so in Fig. 4.

Figs. 4 and 5 bear a close resemblance to the concept of field-induced Bose-Einstein condensation of triplets, which has been under intense scrutiny for several quan-

tum spin-systems recently^{74,75,76,77,78,79,80,81,82,83,84,85,86}. These systems feature a gapful *zero-field* state with the lowest triplet branch 'condensing' as the field is *increased*. For the AFHC, this scenario is reversed, i.e. *decreasing* the field through the critical value for complete polarization B_c , the magnons condense at $q = \pi$ and the system switches from a gapful state to a Luttinger liquid of deconfined spinons. Obviously, the latter does not represent a true gauge-symmetry broken state, since (i) 1D-correlation functions decay algebraically and (ii) the magnons above B_c are constrained by a hard-core repulsion^{87,88,89}.

As the temperature is lowered, the thermal smearing of the approximately quadratic dispersion at $q = \pi$ for $B = B_c$ is reduced, see Figs. 5 c) to d). For the momentum-integrated structure factor this will lead to a critical increase of the density of states at $\omega = 0$ as temperature is lowered. Clear indications of this critical enhancement as $T \rightarrow 0$ have been observed in recent measurements of the transverse relaxation rate T_1^{-1} in nuclear magnetic relaxation experiments at $B = B_c$ on copper pyrazine dinitrate $\text{Cu}(\text{C}_4\text{H}_4\text{N}_2)(\text{NO}_3)_2$ (CuPzN)¹¹.

IV. SUM RULES

Sum rules have been used extensively for the AFHC to evaluate the contribution of 2- and 4-spinon excitations to the spectral weight of the dynamical structure factor at $T=0$ ^{28,33,90,91}. For the present work sum rules can be applied to assess the quality of the analytic continuation. We will focus on the sum rules for the static structure factor $S^{\alpha\beta}(q)$ and the static susceptibility $\chi^{\alpha\beta}(q)$ which obtained by integral transforming the dynamical structure factor⁹³

$$S^{\alpha\beta}(q) = \frac{1}{\pi} \int_0^\infty d\omega (1 + e^{-i\omega t}) S^{\alpha\beta}(q, \omega) \quad (9)$$

$$\chi^{\alpha\beta}(q) = \frac{2}{\pi} \int_0^\infty d\omega \omega^{-1} (1 - e^{-\beta\omega}) S^{\alpha\beta}(q, \omega). \quad (10)$$

While $S^{\alpha\beta}(q, \omega)$ on the right-hand side of eqns. (9) and (10) involve MaxEnt-data, the static structure factor $S^{\alpha\beta}(q)$ in eqn. (9) is calculated from a real-space Fourier transformation of the equal-time correlation functions and the static susceptibility $\chi^{\alpha\beta}(q)$ in eqn. (10) can be evaluated from the Kubo integral

$$\chi^{\alpha\beta}(q) = \sum_r e^{iqr} \int_0^\beta d\tau \langle S_r^\alpha(\tau) S_0^\beta(0) \rangle. \quad (11)$$

of the imaginary time QMC-data. I.e. both, $S^{\alpha\beta}(q)$ and $\chi^{\alpha\beta}(q)$ are obtained from QMC-data which is *independent* from the MaxEnt continuation. In particular the static susceptibility should provide for a clear consistency check regarding the low energy features in the zero field dynamic structure factor at $k = \pi$ as shown in Fig. 3.

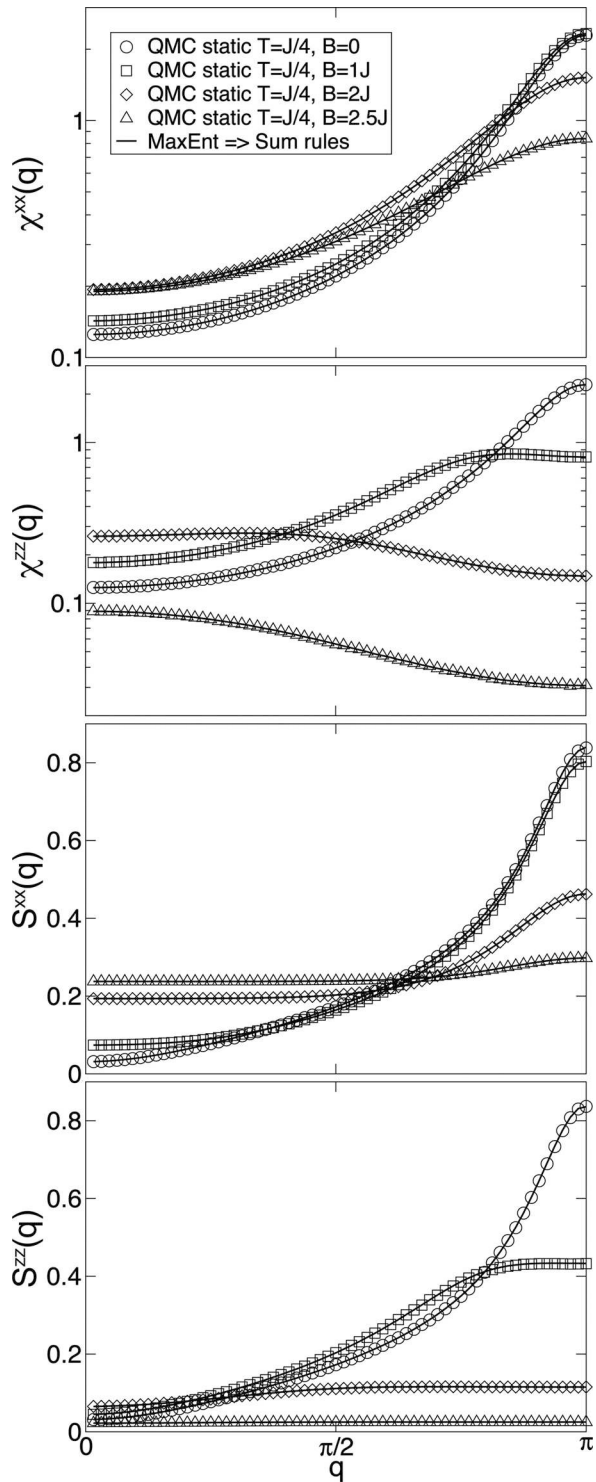


FIG. 6: Comparison of transverse and longitudinal static susceptibility/structure factor (symbols) and sum rules (lines) for $T=J/4$ and four different magnetic fields $B/J = \{0, 1, 2, 2.5\}$ (from top to bottom). All sum rule results are within the error bars of the static quantities which are within symbol size.

In Fig. 6 we compare the left- and right-hand sides of

eqns. (9) and (10) both, for the longitudinal and transverse components, i.e. $\alpha\beta = zz$ and $\alpha\beta = xx$. First, we emphasize that the numerical values for $S^{zz}(0)$, $S^{zz}(\pi)$, $\chi^{zz}(0)$ and $\chi^{zz}(\pi)$ which we have obtained at zero magnetic field are consistent with those reported in refs.^{53,64} and corroborate the parameters of scaling relations⁵³

$$S^{zz}(\pi) = D_s \ln(T_s/T)^{\frac{3}{2}}, \quad D_s = 0.094(1), \quad T_s = 18.3(5)$$

$$\chi^{zz}(\pi) = \frac{D_\chi}{T} \ln(T_\chi/T)^{\frac{1}{2}}, \quad D_\chi = 0.32(1), \quad T_\chi = 5.9(2)$$

for $T = J/4$. Second, Fig. 6 proves an excellent agreement of QMC data involving analytic continuation to that free of the MaxEnt procedure. We have found this agreement for all temperatures and all fields investigated, including those not depicted here. All differences lie within the error bars of the static quantities which is remarkable, given that the typical MaxEnt error is estimated to be $\sim 10\text{-}20\%$ ⁵³. We note that we have performed this sum-rule check for various MaxEnt procedure, i.e. historic, classic, and bryan (see Appendix A) and found the same level of agreement.

V. CONCLUSION

In conclusion, using MaxEnt continuation of QMC results, we have analyzed the evolution of transverse and longitudinal spin excitations of a AFHC with 128 sites at finite temperatures and magnetic fields up to and above the saturation field. Our results are consistent with and complement similar studies using small system ED and zero-temperature BA. In particular we have detailed the difference between longitudinal and transverse excitation as a function of the magnetic field and temperature. Moreover we have considered the field induced magnon 'condensation' at the saturation field and the occurrence incommensurate zero-modes. These investigation may be of relevance to high-field NMR data on AFHC materials¹¹ as well as to inelastic neutron scattering experiments.

Several open questions remain. While the issue of spin-diffusion has been out of reach in this work, future analysis should improve the resolution of the MaxEnt, in order to access the line-shapes at small q . This also pertains to the form of the low- ω spectrum of the zero-field dynamic structure factor at $q = \pi/2$. Finally it will be interesting to perform similar calculations for various generalizations of the AFHC including anisotropy and disorder.

Acknowledgement Part of this research has been funded by the DFG through through Grant No. BR 1084/4-1. W.B. acknowledges the hospitality of the KITP, where this research was supported in part by the NSF under Grant No. PHY05-51164.

APPENDIX A: MAXIMUM ENTROPY METHOD

In this appendix, and for completeness sake, we give a brief account of our MaxEnt approach. In MaxEnt we minimize the functional⁹⁴

$$Q = \frac{1}{2}\chi^2 - \alpha S . \quad (\text{A1})$$

For perfectly uncorrelated QMC data χ^2 is the least-square difference between the data $S^{\alpha\beta}(\tau)$, with standard deviation σ_τ , and the transform of the trial spectrum $A(\omega)$ to imaginary times using the Kernel $K(\omega, \tau)$

$$\chi^2 = \sum_{\tau} \left[\frac{S^{\alpha\beta}(\tau) - \frac{1}{\pi} \int_0^\infty d\omega K(\omega, \tau) A(\omega)}{\sigma_\tau} \right]^2 \quad (\text{A2})$$

where for brevity we disregard the q-dependency. In principle imaginary-time output from the QMC is correlated and needs to be transformed into an eigenbasis of the covariance matrix prior to using eqn. (A2) in order to work with decorrelated data. However, we have observed that diagonalizing the covariance matrix has negligible impact on the spectra which we have analyzed. Therefore we have decided to ignore off-diagonal elements of the covariance matrix.

The second term on the right-hand side of eqn. (A2) contains the Shannon entropy

$$S = \sum_{\omega} \left[A(\omega) - m(\omega) - A(\omega) \ln \left(\frac{A(\omega)}{m(\omega)} \right) \right] , \quad (\text{A3})$$

with respect to a default model $m(\omega)$ which prevents overfitting of the data. We have used a simple flat default

model for all calculations which was iteratively adjusted to match the 0th moment of the trial spectrum. This is different from ref.⁵¹, where several sum-rules have been used to apply additional bias to $A(\omega)$.

The choice of the Lagrange parameter α has been discussed extensively⁹⁴. So-called *classical* and *historic* approaches use Bayesian logic to fix *one* α for the most probable spectrum $A_\alpha(\omega)$. More generally however, a probability distribution $P[\alpha|S^{\alpha\beta}(\tau)]$ exists⁹⁴, which determines the most likely spectrum through the *average*

$$S^{\alpha\beta}(\omega) = \int d\alpha A_\alpha(\omega) P[\alpha|S^{\alpha\beta}(\tau)] . \quad (\text{A4})$$

We have analyzed our results in term of all three ways to choose α . We found classic and averaged spectra to be identical, indicating that $P[\alpha|S^{\alpha\beta}(\tau)]$ is very sharp in our case, which supports the statistical quality of the underlying QMC data. As to be expected, for the historic approach we found somewhat smoother results with a tendency to under-fit the data, thus all shown results are based on averaged spectra.

The minimization of (A1) is done via multi-dimensional Newtown iterations. However, following Bryan's work⁵⁹ we have reduced the effective search directions by a singular value decomposition of the kernel $K = U\Sigma V^T$ down to typically 10-20 of the largest eigenvalues of Σ , depending on the temperature. This leads to a significant speed up of the algorithm.

-
- ¹ K. Ishida, Y. Kitaoka, K. Asayama, M. Azuma, Z. Hiroi, and M. Takano, J. Phys. Soc. Jpn. **63**, 3222 (1994).
² N. Motoyama, H. Eisaki, and S. Uchida, Phys. Rev. Lett. **76**, 3212 (1996).
³ T. Ami, M. K. Crawford, R. L. Harlow, Z. R. Wang, D. C. Johnston, Q. Huang, and R. W. Erwin, Phys. Rev. B **51**, 5994 (1995).
⁴ M. Takigawa, N. Motoyama, H. Eisaki, and S. Uchida, Phys. Rev. Lett. **76**, 4612 (1996).
⁵ D.B. Losee, H.W. Richardson and W.E. Hatfield, J. Chem. Phys. **59**, 3600 (1973).
⁶ C. Broholm, G. Aeppli, Y. Chen, D. C. Dender, M. Enderle, P. R. Hammar, Z. Honda, K. Katsumata, C. P. Landee, M. Oshikawa, L. P. Regnault, D. H. Reich, S. M. Shapiro, M. Sieling, M. B. Stone, M. M. Turnbull, I. Zaliznyak, and A. Zheludev, p 211-234 in *High Magnetic Fields - applications in condensed matter physics and spectroscopy* C. Berthier, L.P. Lévy, and G. Martinez, Eds. Springer Verlag (2002).
⁷ M. B. Stone, D. H. Reich, C. Broholm, K. Lefmann, C. Rischel, C. P. Landee, and M. M. Turnbull, Phys. Rev. Lett. **91**, 037205 (2003).
⁸ M. Takigawa, O. A. Starykh, A. W. Sandvik, and R. R. P. Singh, Phys. Rev. B **56**, 13681 (1997).
⁹ K. R. Thurber, A. W. Hunt, T. Imai, and F. C. Chou, Phys. Rev. Lett. **87**, 247202 (2001).
¹⁰ A. U. B. Wolter, P. Wzietek, S. Süllow, F.J. Litterst, A. Honecker, W. Brenig, R. Feyerherm, and H.-H. Klauss, Phys. Rev. Lett. **94**, 057204 (2005).
¹¹ H. Kühne, H.-H. Klauss, S. Grossjohann, W. Brenig, F. Litterst, A. Reyes, P. Kuhns, M. Turnbull, and C. Landee, cond-mat arXiv:0804.2170 (2008).
¹² F. L. Pratt, S. J. Blundell, T. Lancaster, C. Baines, and S. Takagi, Phys. Rev. Lett. **96**, 247203 (2006).
¹³ F. Heidrich-Meisner, A. Honecker, and W. Brenig, Eur. Phys. J. Special Topics **151**, 135 (2007).
¹⁴ A. V. Sologubenko, T. Lorenz, H. R. Ott, and A. Freimuth, J. Low. Temp. Phys. **147**, 387 (2007).
¹⁵ H. Bethe, Z. Phys. **71**, 205 (1931).
¹⁶ L. D. Faddeev and L. A. Takhtajan, Phys. Lett. A **85**, 375 (1981).
¹⁷ A. Klümper, Z. Phys. B **91**, 507 (1993).
¹⁸ D. C. Johnston, R. K. Kremer, M. Troyer, X. Wang, A. Klumper, S. L. Bud'ko, A. F. Panchula, and P. C. Canfield,

- Phys. Rev. B **61**, 9558 (2000).
- 19 A. Klümper and D. C. Johnston, Phys. Rev. Lett. **84**, 4701 (2000).
 - 20 J. des Cloizeaux and J. J. Pearson, Phys. Rev. **128**, 2131 (1962).
 - 21 T. Yamada, Prog. Theor. Phys. **41**, 880 (1969).
 - 22 G. Müller, H. Thomas, H. Beck, and J. C. Bonner, Phys. Rev. B **24**, 1429 (1981).
 - 23 J. C. Bonner and H. W. J. Blöte, Phys. Rev. B **25**, 6959 (1982).
 - 24 K. Lefmann and C. Rischel, Phys. Rev. B **54**, 6340 (1996).
 - 25 T. D. Kuhner and S. R. White, Phys. Rev. B **60**, 335 (1999).
 - 26 D. Gobert, C. Kollath, U. Schollwöck, and G. Schutz, Phys. Rev. E **71**, 036102 (2005).
 - 27 A. H. Bougourzi, M. Couture, and M. Kacir, Phys. Rev. B **54**, R12669 (1996).
 - 28 M. Karbach, G. Müller, A. H. Bougourzi, A. Fledderjohann, and K. H. Mütter, Phys. Rev. B **55**, 12510 (1997).
 - 29 A. H. Bougourzi, M. Karbach, and G. Müller, Phys. Rev. B **57**, 11429 (1998).
 - 30 A. H. Bougourzi, Mod. Phys. Lett. B **10**, 1237 (1996).
 - 31 A. Abadaa, A. H. Bougourzi, and B. Si-Lakhala, Nucl. Phys. B **497**, 733 (1997).
 - 32 B. S. Lakhala and A. Abadab, Physica B **369**, 196 (2005).
 - 33 J. S. Caux and R. Hagemans, J. Stat. Mech. p. P12013 (2006).
 - 34 N. Kitanine, J. M. Maillet, and V. Terras, Nucl. Phys. B **567**, 554 (2000).
 - 35 J. S. Caux, R. Hagemans, and J. M. Maillet, J. Stat. Mech.: Theor. and Expm. **123**, 9003 (2005).
 - 36 D. Biegel, M. Karbach, and G. Müller, Europhys. Lett. **59**, 882 (2002).
 - 37 D. Biegel, M. Karbach, and G. Müller, J. Phys. A: Math. Gen. **36**, 5361 (2003).
 - 38 J. Sato, M. Shiroishi, and M. Takahashi, J. Phys. Soc. Jp. **73**, 3008 (2004).
 - 39 M. Karbach and G. Müller, Phys. Rev. B **62**, 14871 (2000).
 - 40 J.-S. Caux and J. M. Maillet, Phys. Rev. Lett. **95**, 077201 (2005).
 - 41 H. J. Schulz, Phys. Rev. B **34**, 6372 (1986).
 - 42 M. Pustilnik, M. Khodas, A. Kamenev, and L. I. Glazman, Phys. Rev. Lett. **96**, 196405 (2006).
 - 43 R. G. Pereira, J. Sirker, J.-S. Caux, R. Hagemans, J. M. Maillet, S. R. White, and I. Affleck, Phys. Rev. Lett. **96**, 257202 (2006).
 - 44 R. G. Pereira, J. Sirker, J.-S. Caux, R. Hagemans, J. M. Maillet, S. R. White, and I. Affleck, J. Stat. Mech. p. P08022 (2007).
 - 45 K. Fabricius, U. Löw, and J. Stolze, Phys. Rev. B **55**, 5833 (1997).
 - 46 K. Fabricius and B. M. McCoy, Phys. Rev. B **57**, 8340 (1998).
 - 47 F. Heidrich-Meisner, A. Honecker, D. C. Cabra, and W. Brenig, Phys. Rev. B **68**, 134436 (2003).
 - 48 J. Sirker and A. Klümper, Phys. Rev. B **71**, 241101(R) (2005).
 - 49 J. Sirker, Phys. Rev. B **73**, 224424 (2006).
 - 50 M. Jarrell, *et al.*, Phys. Rep. **269**, 133 (1996).
 - 51 J. Deisz, M. Jarrell, and D. L. Cox, Phys. Rev. B **42**, 4869 (1990).
 - 52 J. Deisz, M. Jarrell, and D. L. Cox, Phys. Rev. B **48**, 10227 (1993).
 - 53 O. A. Starykh, A. W. Sandvik, and R. R. P. Singh, Phys. Rev. B **55**, 14953 (1997).
 - 54 S. Grossjohann and W. Brenig, unpublished.
 - 55 A.W. Sandvik and J. Kurkijärvi, Phys. Rev. B **43**, 5950 - 5961 (1991).
 - 56 O.F. Syljuåsen and A.W. Sandvik, Phys. Rev. E **66**, 046701 (2002).
 - 57 A.W. Sandvik, J. Phys. A: Math. Gen. **25**, 3667 (1992).
 - 58 A. Dorneich and M. Troyer, Phys. Rev. E **64**, 066701 (2001).
 - 59 J. Skilling and R.K. Bryan, Mon. Notices R. Astron. Soc. **211**:111-124 (1984).
 - 60 T. Yamada, Prog. Theor. Phys. Jpn. **41**, 880 (1969).
 - 61 J. des Cloizeaux and J.J. Pearson, Phys. Rev. **128**, 2131 (1962).
 - 62 N. Bloembergen, Physica (Amsterdam) **15**, 386 (1949).
 - 63 P.G. de Gennes, J. Phys. Chem. Solids **4**, 223 (1958).
 - 64 Y.J. Kim, M. Greven, U.-J. Wiese and R.J. Birgenau, Eur. Phys. J. B **4**, 291 (1998).
 - 65 L.N. Bulaevskii, Sov. Phys. JETP **16**, 685 (1963)
 - 66 S. Inawashiro and S. Katsura, Phys. Rev. **140**, A 892 (1965).
 - 67 A.J. Silverstein and Z.G. Soos, J. Chem. Phys. **53**, 326 (1970).
 - 68 M.D. Johnson and M. Fowler, Phys. Rev. B **34**, 1728 (1986).
 - 69 J.B. Parkinson and J.C. Bonner, Phys. Rev. B. **32**, 4703 (1985).
 - 70 J.P. Groen, T.O. Klaassen, N.J. Poulis, G. Müller, H. Thomas and H. Beck, Phys. Rev. B **22**, 5369 (1980).
 - 71 E. Pytte, Phys. Rev. B **10**, 4637 (1974).
 - 72 N. Ishimura and H. Shiba, Prog. Theor. Phys. Jpn. **57**, 1862 (1977).
 - 73 M. Karbach, K.-H. Mütter and M. Schmidt, J. Phys.: Condens. Matter **7**, 2829 (1995).
 - 74 T. Nikuni, M. Oshikawa, A. Oosawa, and H. Tanaka, Phys. Rev. Lett. **84**, 5868 (2000).
 - 75 A. Oosawa, H. A. Katori and H. Tanaka, Phys. Rev. B **63**, 134416 (2001).
 - 76 C. Rüegg, N. Cavadini, A. Furrer, H.-U. Gütler, K. Krüger, H. Mutka, A. Wildes, K. Habicht and P. Vorderwisch, Nature **423**, 62 (2003).
 - 77 G. Misguich and M. Oshikawa, *et al.*, J. Phys. Soc. Jpn. **73** 3429 (2004).
 - 78 S. E. Sebastian, N. Harrison, C. D. Batista, L. Balicas, M. Jaime, P. A. Sharma, N. Kawashima and I.R. Fisher, Nature **441**, 617 (2006).
 - 79 G. Chaboussant, P. A. Crowell, L. P. Lévy, O. Piovesana, A. Madouri and D. Maily, Phys. Rev. B. **55**, 3046 (1997).
 - 80 B. C. Watson, V. N. Kotov, M. W. Meisel, D. W. Hall, G. E. Granroth, W. T. Montfrooij, S. E. Nagler, D. A. Jensen, R. Backov, M. A. Petruska, G. E. Fanucci and D. R. Talham, Phys. Rev. Lett. **86**, 5168 (2001).
 - 81 T. Lorenz, O. Heyer, M. Garst, F. Anfuso, A. Rosch, Ch. Rüegg and K. Krüger, Phys. Rev. Lett. **100**, 067208 (2008).
 - 82 Z. Honda, H. Asakawa and K. Katsumata, Phys. Rev. Lett. **81**, 2566 (1998).
 - 83 V. S. Zapf, D. Zocco, B. R. Hansen, M. Jaime, N. Harrison, C. D. Batista, M. Kenzelmann, C. Niedermayer, A. Lacerda and A. Paduan-Filho, Phys. Rev. Lett. **96**, 077204 (2006).
 - 84 S. A. Zvyagin, J. Wosnitza, C. D. Batista, M. Tsukamoto, N. Kawashima, J. Krzystek, V. S. Zapf, M. Jaime, N. F. Oliveira, Jr., and A. Paduan-Filho, Phys. Rev. Lett. **98**,

- 047205 (2007).
- ⁸⁵ H. Manaka, I. Yamada, Z. Honda, H. Aruga Katori and K. Katsumata, *J. Phys. Soc. Jpn.* **67**, 3913 (1998).
- ⁸⁶ V. O. Garlea, A. Zheludev, T. Masuda, H. Manaka, L.-P. Regnault, E. Ressouche, B. Grenier, J.-H. Chung, Y. Qiu, K. Habicht, K. Kiefer and M. Boehm, *Phys. Rev. Lett.* **98**, 167202 (2007).
- ⁸⁷ I. Affleck, *Phys. Rev. B* **41**, 6697 (1990); **43**, 3215 (1991).
- ⁸⁸ E. S. Sorensen and I. Affleck, *Phys. Rev. Lett.* **71**, 1633 (1993).
- ⁸⁹ T. Giamarchi and A. M. Tsvelik, *Phys. Rev. B* **59**, 11398 (1999).
- ⁹⁰ B.Si Lakhali and A. Abada, *Physica B* 369, 196 - 208 (2005).
- ⁹¹ B.Si Lakhali and A. Abada, *J. Phys. A: Math. Gen.* 37, 497 (2005).
- ⁹² A.W. Sandvik, *Phys. Rev. B* **52**, R9831 (1995).
- ⁹³ P.C. Hohenberg and W. F. Brinkman, *Phys. Rev. B* **10**, 128 (1974).
- ⁹⁴ J.E. Gubernatis, M. Jarrell, R.N. Silver and D.S. Sivia, *Phys. Rev. B* **44**, 6011 (1991).
- ⁹⁵ X. Zotos, *J. Low Temp. Phys.* **126**, 1764 (1999).
- ⁹⁶ J.V. Alvarez and C. Gros, *Phys. Rev. B* **66**, 094403 (2002).
- ⁹⁷ B.N. Narozhny, A.J. Millis and N. Andrei, *Phys. Rev. B* **58**, R2921 (1998).
- ⁹⁸ S. Fujimoto and N. Kawakami, *Phys. Rev. Lett.* **90**, 197202 (2003).